PHOTONICS Research

Mid-infrared Q-switch performance of ZrC

Yangyang Liang,[1] Tao Li,[1,2,3,*] Wenchao Qiao,[2] Tianli Feng,[2,6] Shengzhi Zhao,[2] Yuefeng Zhao,[3,4] Yuzhi Song,[3,4] and Christian Kränkel[5]

[1]China Key Laboratory of Laser & Infrared System (Shandong University), Ministry of Education, Qingdao 266237, China
[2]School of Information Science and Engineering, and Shandong Provincial Key Laboratory of Laser Technology and Application, Shandong University, Qingdao 266237, China
[3]Collaborative Innovation Center of Light Manipulations and Applications, Shandong Normal University, Jinan 250358, China
[4]School of Physics and Electronics, Shandong Normal University, Jinan 250358, China
[5]Leibniz-Institut für Kristallzüchtung, 12489 Berlin, Germany
[6]e-mail: tlfeng@sdu.edu.cn
*Corresponding author: litao@sdu.edu.cn

Received 26 June 2020; revised 21 August 2020; accepted 21 August 2020; posted 29 September 2020 (Doc. ID 401168); published 19 November 2020

Zirconium carbide (ZrC) with layered structure and nanoparticle morphology was prepared by sonication in an ethyl alcohol solvent. The morphology and saturable absorption properties of the ZrC were systematically analyzed. By using ZrC nanoparticle coated substrates as saturable absorbers, stable *Q*-switched 3 μm Er:Lu_2O_3 lasers were realized. Pulse durations of 50 ns with pulse energies of 20 μJ and peak power of 0.4 kW are the shortest obtained with novel-material-based *Q*-switched lasers in the 3 μm wavelength range.

https://doi.org/10.1364/PRJ.401168

1. INTRODUCTION

Benefiting from the spectral absorption of water peaking at 2.94 μm with an absorption length of only 1 μm, mid-infrared (IR) lasers around 3 μm are highly demanded for applications in laser surgery, ophthalmology, and chemical sensing [1]. Laser emission in this range can be generated by optical parametric oscillators (OPOs) [1–3], antimonide-based heterojunction laser diodes [1,4,5], Raman-shifted lasers [6], transition-metal-doped II-VI chalcogenide lasers (Cr^{2+}, Fe^{2+}) [7,8], and also by rare-earth-doped lasers (Er^{3+} [9–11], Ho^{3+} [12], and Dy^{3+} [13]). Among these, Er^{3+}-based solid-state lasers are widely used cost efficient lasers in the range of 2.58–2.94 μm with the advantages of compactness, high efficiency, good stability, and long operation lifetime. In particular, a slope efficiency as high as 41% was obtained from a 3 at.% Er:SrF_2 bulk laser. This is much higher than the theoretical limit given by the Stokes efficiency of 35% and enabled by an upconversion process recycling excitation from the lower laser level [14]. The cubic sesquioxides (Y_2O_3, Lu_2O_3, and Sc_2O_3) providing much better thermo-mechanical properties than, e.g., SrF_2 and low phonon energies for oxide materials, are suitable host materials for 3 μm lasers [15]. For example, a continuous wave (CW) Er:Lu_2O_3 laser delivered the highest output power of 5.9 W of any Er^{3+}-doped laser operated at room temperature [9]. Also, ceramic Er:Lu_2O_3 is very promising and up to now delivered an output power of 2.6 W under 11.2 W of pump power in CW operation [11]. Further improvement of the average output power is feasible by operating the laser at liquid nitrogen temperatures. Under these conditions, the thermal conductivity of sesquioxides increases by nearly an order of magnitude, which enabled a record output power of 14 W at 2.7 μm in a 2 at.% Er:Y_2O_3 ceramic laser under a high pump power of 56 W. In this case, the slope efficiency amounted to ~26% [16].

In the past decade, numerous two-dimensional (2D) materials were widely explored and extensively investigated as novel types of passive optical modulators. These studies revealed the outstanding ability of 2D materials in generating 3 μm IR laser pulses [17,18]. The 244 ns pulses were realized in a graphene *Q*-switched ceramic Er:Lu_2O_3 laser [11]; a MoS_2 *Q*-switched Er:Lu_2O_3 laser enabled 335 ns pulses [16], and pulses as short as 194 ns were obtained from a black phosphorus *Q*-switched Ho, Pr:$LuLiF_4$ (Ho,Pr:LLF) laser [19]. Even though a $TiSe_2$ *Q*-switched Ho,Pr:LLF laser yielded an even shorter pulse duration of 160.5 ns [18], the reported results were still inferior to those achieved with conventional bulk modulators. For example, *Q*-switched with Fe^{2+}:ZnSe, an Er:$Y_3Al_5O_{12}$ (Er:YAG) laser emitted 50 ns laser pulses [20]. By using active *Q*-switching based on an electro-optic modulator, the laser can emit even shorter pulses of 25.2 ns [21].

Besides some layered materials, fewer studied bulk materials have turned out to be suitable modulator materials for *Q*-switching and even mode-locking of lasers [22]. Recently, a bulk-structured WTe_2-based saturable absorber (SA) consisting of hundreds of monolayers cohered by van der Waals forces enabled stable mode-locking of an Er-doped fiber at 1556 nm

with pulse durations of 770 fs [23]. Thus, other layer materials in a bulk-structured multi-layer arrangement could also be promising optical modulators. Zirconium carbide (ZrC) is one of the potential candidates from this family, which exhibits many outstanding electronical properties. Compared with well-studied low-dimensional materials such as graphene, MoS_2, black phosphorus, carbon nanotubes, $Cu_{1.8}Se$, and $TiSe_2$, ZrC comprises a mixture of covalent, metallic, and ionic bonds [24], which leads to various interactions between photons and electrons and further results in unique properties. Therefore, ZrC-based SAs should be very promising candidates for optical modulators in the 3 μm wavelength region. In this paper, the band structure of ZrC was analyzed in detail, proving the existence of optical absorption in the 3 μm wavelength region. Nanoparticle cluster structure samples were prepared and compared with nanoflake structures in morphology and saturable absorption properties. By employing ZrC-nanoparticle-clusters-based SAs in an $Er:Lu_2O_3$ laser, stable passively *Q*-switched (PQS) lasers with tens of nanoseconds (ns) pulse duration were realized. Under a pump power of 10.9 W at 976 nm, laser pulses as short as 50 ns were generated at a repetition rate of 13 kHz with an average output power of 262 mW, corresponding to pulse energy and peak power of 20 μJ and 0.4 kW, respectively. To the best of our knowledge, these are the shortest pulse durations and highest peak power levels of all novel-material-based *Q*-switched lasers in the 3 μm wavelength range.

2. BAND STRUCTURE, PREPARATION, AND CHARACTERIZATION OF ZrC SATURABLE ABSORBERS

First-principle calculations were performed based on an optimized ZrC face-centered cubic unit cell [Fig. 1(a)] in the Vienna ab-initio simulation package (VASP) code by using the generalized gradient approximation with the Perdew–Burke–Ernzerhof (PBE) exchange-correlation functional and the projected augmented wave (PAW) approach with a plane wave cutoff energy of 340 eV [25] along the high-symmetry direction in the Brillouin zone. The resulting cubic Fm-3m unit cell with a lattice parameter of 4.700 Å is in good agreement with the results reported in Ref. [26]. The calculated results of the electric band structure and densities of states (DOS) including projected DOS (PDOS) are visualized in Figs. 1(b) and 1(c). These graphs confirm a metallic nature of ZrC with a DOS at the Fermi level at 0 eV of 0.5 contributed by the Zr atom. Further, the PDOS in Fig. 1(c) has also revealed the existence of covalent bonds [27]. Similar to graphene [28], the interband and intraband processes of metallic ZrC are responsible for its broadband absorption properties, and the 3 μm wavelength region is included.

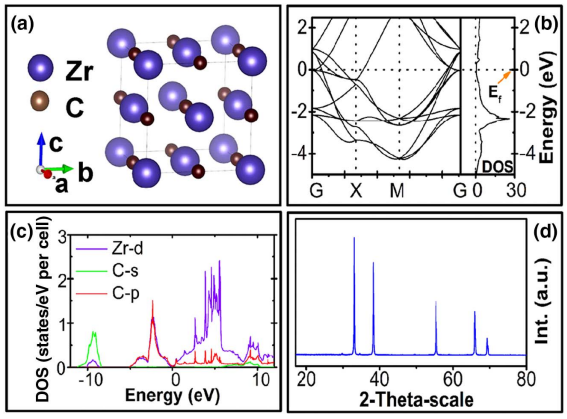

Fig. 1. (a) Scheme of the face-centered cubic ZrC unit cell, (b) calculated band structure of ZrC, (c) projected DOS for ZrC, and (d) XRD pattern of ZrC powder.

The precursors of the fabricated ZrC nanoclusters and nanoflakes are commercial ZrC powders. The result of the X-ray diffraction (XRD) analysis of these powders is shown in Fig. 1(d). It confirms the face-centered cubic structure of ZrC [29] and is in good agreement with the VASP calculation.

By sonication in solvent, the chemical bonds of bulk ZrC can be efficiently broken, and dispersed nanoflakes and nanoparticles are formed. During the preparation process, 14 mg ZrC powder was sonicated for 4 h in 7 mL pure ethyl alcohol solvent. Scanning electron microscopy (SEM) and transmission electron microscopy (TEM) images of the deposited suspensions are shown in Figs. 2(a) and 2(b). Bulk pieces, nanoparticles, nanoparticle clusters, and even some nanosheets could be observed. For stratification, the suspension was treated by differential centrifugation at 9000 r/min for 5 min first; then the solvent was divided in three parts of 5, 1, and 1 mL from top to bottom, corresponding to a sample containing layered material, bulk material, and the sediments, respectively. Finally, the top 5 mL supernatant was again centrifuged at 12,000 r/min for another 5 min, and the top 3 mL supernatant was collected, while the medium 1 mL was subject to natural sedimentation. Nanoparticles and nanoflakes were collected from supernatants

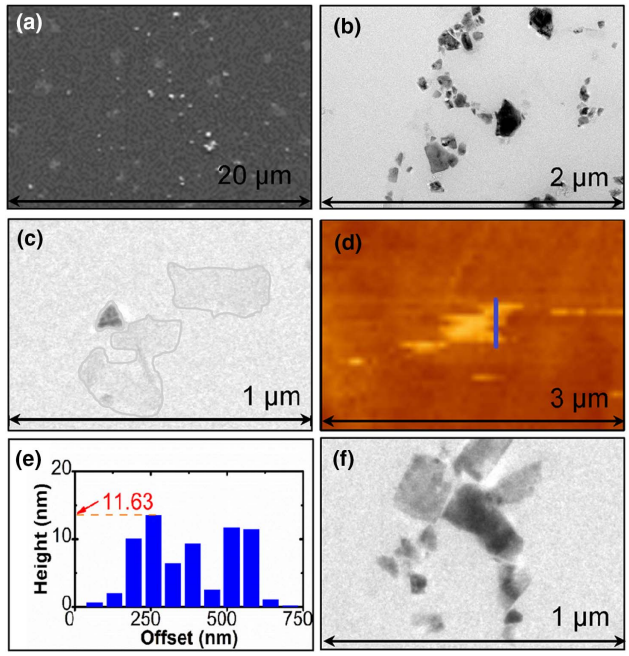

Fig. 2. (a) SEM image and (b) TEM image of sonicated ZrC solvent; (c) TEM image, (d) AFM image, and (e) height variations in the region marked in blue in (d) of ZrC nanoflakes; (f) TEM image of a ZrC cluster.

of the middle 1 mL and the 3 mL recentrifuged suspension. As a reference experiment, well-studied MoS_2 was prepared and treated in the same process. TEM and atomic force microscopy (AFM) images of ZrC nanoflakes are shown in Figs. 2(c) and 2(d), and the height distribution is shown in Fig. 2(e). These results reveal the presence of nanoflakes with dimensions of hundreds of nanometers and a height around 10 nm, and the average roughness of this sample was measured to be 3.1 nm. A TEM image of a nanoparticle cluster is shown in Fig. 2(f), from which a similar size of hundreds of nanometers can be seen. An SA containing nanoflakes was prepared on a YAG substrate (12.7 mm × 1 mm) by spin coating, while the SA containing ZrC clusters was prepared by dropping 5 μL solvent on a similar substrate. Reference samples of MoS_2 were prepared through the same treatment.

The linear transmission of both ZrC SAs in the wavelength range between 2000 and 3200 nm was characterized by a UV-visible (VIS)-near-IR (NIR) spectrophotometer (Cary 5000, Agilent Technologies Co., Ltd.). The transmittance of both samples at the laser wavelength of 2845 nm in our experiments [see Figs. 3(a) and 3(b)] amounts to 80.1% and 66.9% for the nanoflakes and nanocluster ZrC SA, respectively. The fluctuations in the transmission signal at around 2.7 μm are caused by atmospheric absorption. The nonlinear transmission of our SA sample at this wavelength was determined by a home-built *Q*-switched laser with pulse duration of 50 to 80 ns at a wavelength of 2845 nm. From the data depicted in Figs. 3(c) and 3(d), the saturation intensity and modulation depth as well as the nonsaturable losses were fitted to be around 1.3 MW/cm^2, 3.2%, and 15.7%, respectively. In contrast, the nanocluster sample shows a much larger modulation depth of 10% at an order of magnitude higher saturation intensity of 12.5 MW/cm^2 and nonsaturable losses of ~24%. It should be noted that the nonsaturable losses to a large part result from the Fresnel losses at the YAG plate and can be reduced by the use of Brewster geometry or antireflection (AR) coatings. However, the rough surface of the SAs is also contributed by scattering losses. As a consequence, one can expect much larger pulse energies and significantly reduced pulse duration at the largest pump powers by using the ZrC nanocluster SA.

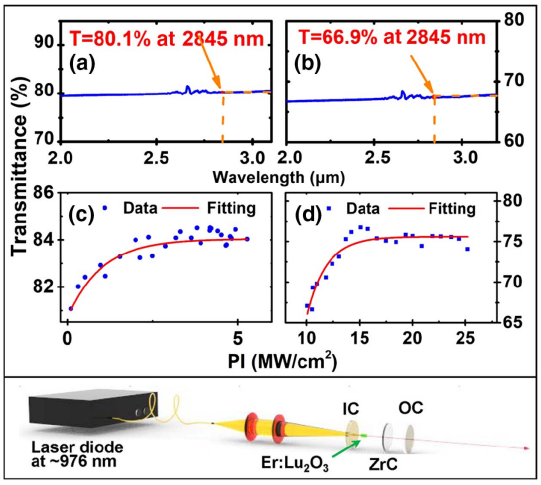

Fig. 3. Top: linear transmission of (a) ZrC nanoflake SA and (b) ZrC nanocluster SA, nonlinear transmission of (c) ZrC nanoflake SA and (d) ZrC nanocluster SA; bottom: laser configuration scheme.

3. LASER EXPERIMENTS

A. Experimental Setup

The setup of our ZrC-*Q*-switched Er:Lu_2O_3 laser is sketched in the bottom of Fig. 3. The 2.5 cm long concave-plane cavity consisted of an input coupler (IC) and an output coupler (OC). The IC mirror was a concave dichroic fused silica mirror (R = 1000 mm), AR coated for the pump wavelength of 976 nm, and high-reflection (HR) coated for possible laser wavelengths between 2.7 and 2.9 μm. As an OC mirror, we used different flat mirrors on YAG substrates with transmissions of 1%, 3%, and 5% at the laser wavelength. An uncoated 3 mm × 3 mm × 10 mm Er:Lu_2O_3 crystal with a doping concentration of 7 at.% was employed as the gain medium. The crystal was wrapped in indium foil and mounted on a copper block water-cooled to 13°C. The pump light was supplied by a volume Bragg grating stabilized fiber-coupled laser diode emitting at 976 nm with a numerical aperture of 0.15 and a fiber core diameter of 105 μm. The pump beam was focused onto the end-face of the crystal with a diameter of 200 μm. The single-pass absorption efficiency was measured to be 89.5%. The output power and laser spectrum were measured by a power meter (PM 200 with SC 470C power head, Thorlabs Inc.) and a grating spectrometer (Omni-λ300, Zolix, China), respectively. The pulse train was detected by a fast HgCdTe IR detector with a response time of 1 ns (PVI-4TE-4, Vigo System S.A.) and visualized by a digital oscilloscope with a rise time of 350 ps (1 GHz bandwidth and 5 GHz sampling rate, DPO 7104C, Tektronix Inc.). The beam quality of the laser was determined by the 90/10 scanning knife-edge method.

B. CW and *Q*-Switched Laser Performance

CW laser operation was realized without the SA in the cavity. As shown in Fig. 4(a), the threshold pump powers were mea-

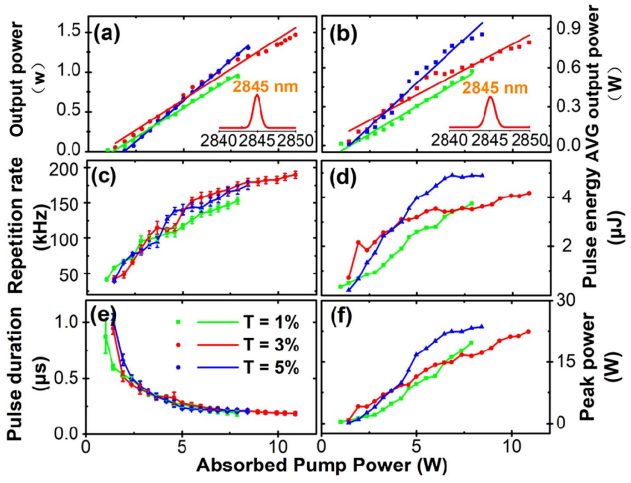

Fig. 4. (a) Output power versus pump power of the CW laser (inset: CW lasing spectrum); (b) output power (inset: lasing spectrum), (c) repetition rate, (d) pulse energy, (e) pulse duration, and (f) peak power versus absorbed pump power for the ZrC nanoflakes SA *Q*-switched laser.

sured to be 0.74, 0.98, and 1.77 W at OC transmissions of 1%, 3%, and 5%, respectively. To protect the crystal from damage, the absorbed pump powers were limited to 7.9, 10.9, and 8.4 W at $T = 1\%$, 3%, and 5%. Under these pump powers, maximum output powers of 0.94, 1.48, and 1.30 W were achieved, respectively, at slope efficiencies of 15%, 15%, and 20%, respectively. The emission wavelength was centered at 2845 nm [inset of Fig. 4(a)], and the M^2 factor was determined to be 1.6/1.7 in the tangential/sagittal plane.

By inserting the nanoflake ZrC-SA into the cavity, stable Q-switching was realized. As depicted in Fig. 4(b), the thresholds of the absorbed pump power of the stable Q-switched lasers were found at 0.67, 1.04, and 1.12 W at $T = 1\%$, 3%, and 5%, respectively. It should be noted that the Fresnel reflection of the YAG substrate of the SA caused a sub-cavity, which increased the total feedback in the cavity, yielding lower thresholds for Q-switched operation as compared to CW operation. Under absorbed pump powers of 7.9, 10.9, and 8.4 W, average output powers of 0.57, 0.79, and 0.85 W were achieved at $T = 1\%$, 3%, and 5%, corresponding to slope efficiencies of 9%, 8%, and 14%, respectively. As shown in the inset of Fig. 4(b), the peak emission wavelength remained unchanged at 2845 nm, and the M^2 factor was only slightly increased to 1.8/1.9 in the tangential/sagittal plane at the maximum average output power. Detailed characteristics of the Q-switched pulses are provided in Figs. 4(c)–4(f). The repetition rates increased with the absorbed pump power, and the highest repetition rates were 153, 186, and 175 kHz at $T = 1\%$, 3%, and 5%, respectively. The highest pulse energies were calculated to be 3.7, 4.2, and 4.9 μJ, respectively. The pulse durations decreased with increasing pump power, and the shortest pulse durations were measured to be 190, 185, and 208 ns at $T = 1\%$, 3%, and 5%, respectively. As a result, the maximum peak powers were calculated to be 20, 22, and 24 W.

In further experiments, we utilized the nanocluster SA to obtain Q-switching and obtained substantially shorter pulse durations. Reflection, absorption, and scattering of the nanoclusters increased the total cavity losses [cf. Figs. 3(b) and 3(d)], which significantly increased the laser threshold. To protect the laser crystal against damage at the required pump powers, the output properties with this SA were only investigated using the 3% OC. Stable Q-switched laser operation was realized. As shown in Fig. 5(a), under a pump power of 10.9 W, a maximum average output power of 262 mW was obtained, corresponding to a slope efficiency of 13%. In a 20 min measurement, we determined the minimum–maximum output instability to be ~12%. The detailed characteristics of these pulses are shown in Fig. 5. Under the maximum pumping power of 10.9 W, the shortest pulse durations of 50 ns were achieved, yielding pulse energy of 22 μJ and peak power of 0.4 kW. In Fig. 5(d), the linear increase of the pulse energy is displayed, so we believe the pulse energy is still unsaturated under the current pumping level. However, we did not further enhance the pump level since the IC will be damaged under a higher pump power [see inset of Fig. 5(a)]. To the best of our knowledge, these are the highest peak powers and shortest pulse durations obtained from any novel material Q-switched laser in the 3 μm range. Using the MoS_2 cluster SA, Q-switched lasers

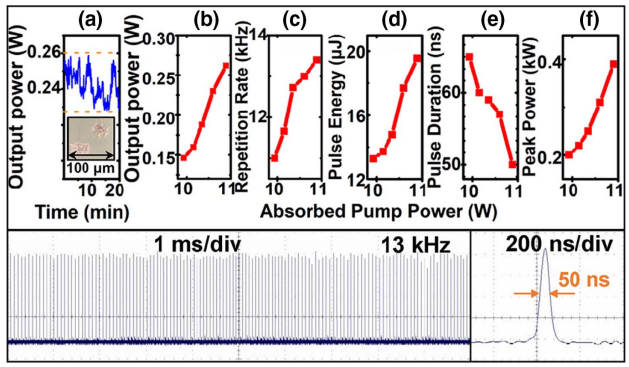

Fig. 5. Top: (a) output stability of the nanocluster SA Q-switched laser operation (inset: image of damaged IC) as well as (b) output power, (c) repetition rate, (d) pulse energy, (e) pulse duration, and (f) peak power versus absorbed pump power; bottom: typical Q-switched pulse train and temporal pulse shape at the maximum average output power.

with similar repetition rate could be realized. In this case, the pulse durations amounted to 120 ns, which is one-third of the pulse achieved with a nanoflake-based SA [10], although the main peak was always accompanied by sidelobes. Our results reveal that cluster-based films are of great potential in shorter pulse delivering in comparison with nanoflake-based films, and, in future experiments, higher OC transmissions could pave the way to few-ns pulse durations from 2D material Q-switched Er-doped lasers emitting around 3 μm.

4. CONCLUSION

In conclusion, we demonstrated first-principle calculations confirming that metallic ZrC can be an outstanding optical modulator for mid-IR lasers. ZrC nanofilms and nanoclusters were successfully exfoliated from commercial powder by sonication. By employing a ZrC nanoflakes SA as a modulation device, a PQS Er:Lu_2O_3 laser with a maximum peak power of 24 W was realized under a pump power of 10.9 W. A ZrC-nanoparticle-cluster-based SA delivered even shorter pulses of 50 ns duration at a repetition rate of 13 kHz with a pulse energy of 22 μJ and a peak power of 0.4 kW. To the best of our knowledge, these are the shortest pulses and highest peak powers from any novel material-based Q-switched laser in the 3 μm range. The results validate that ZrC is a suitable SA for generating shortest Q-switched pulse durations in the mid-IR spectral range.

Funding. National Key Research and Development Program of China (2016YFB1102201); Taishan Young Scholar Program of Shandong Province (tsqn201812010); National Natural Science Foundation of China (61605100); Qi Lu Young Scholars Program of Shandong University (Tao Li, Tianli Feng); Young Scholars Program of Shandong University (Wenchao Qiao).

Disclosures. The authors declare no conflicts of interest.

REFERENCES

1. A. Godard, "Infrared (2–12 μm) solid-state laser sources: a review," C. R. Phys. **8**, 1100–1128 (2007).
2. Y. Jin, S. M. Cristescu, F. J. Harren, and J. Mandon, "Broadly, independent-tunable, dual-wavelength mid-infrared ultrafast optical parametric oscillator," Opt. Express **23**, 20418–20427 (2015).
3. P. Jiang, T. Chen, D. Yang, B. Wu, S. Cai, and Y. Shen, "A fiber laser pumped dual-wavelength mid-infrared optical parametric oscillator based on aperiodically poled magnesium oxide doped lithium niobate," Laser Phys. Lett. **10**, 115405 (2013).
4. D. Z. Garbuzov, H. Lee, V. Khalfin, R. Martinelli, J. C. Connolly, and G. L. Belenky, "2.3–2.7-μm room temperature CW operation of InGaAsSb-AlGaAsSb broad waveguide SCH-QW diode lasers," IEEE Photon. Technol. Lett. **11**, 794–796 (1999).
5. A. Bauer, K. Rößner, T. Lehnhardt, M. Kamp, S. Höfling, L. Worschech, and A. Forchel, "Mid-infrared semiconductor heterostructure lasers for gas sensing applications," Semicond. Sci. Technol. **26**, 014032 (2011).
6. G. Zhu, L. Geng, X. Zhu, L. Li, Q. Chen, R. A. Norwood, T. Manzur, and N. Peyghambarian, "Towards ten-watt-level 3–5 μm Raman lasers using tellurite fiber," Opt. Express **23**, 7559–7573 (2015).
7. V. V. Fedorov, S. B. Mirov, A. Gallian, D. V. Badikov, M. P. Frolov, Y. V. Korostelin, V. I. Kozlovsky, A. I. Landman, Y. P. Podmar'kov, V. A. Akimov, and A. A. Voronov, "3.77–5.05-μm tunable solid-state lasers based on Fe^{2+}-doped ZnSe crystals operating at low and room temperatures," IEEE J. Quantum Electron. **42**, 907–917 (2006).
8. S. B. Mirov, V. V. Fedorov, D. Martyshkin, I. S. Moskalev, M. Mirov, and S. Vasilyev, "Progress in mid-IR lasers based on Cr and Fe-doped II-VI chalcogenides," IEEE J. Sel. Top. Quantum Electron. **21**, 292–310 (2015).
9. T. Li, K. Beil, C. Kränkel, and G. Huber, "Efficient high-power continuous wave Er:Lu_2O_3 laser at 2.85 μm," Opt. Lett. **37**, 2568–2570 (2012).
10. M. Fan, T. Li, S. Zhao, G. Li, H. Ma, X. Gao, C. Kränkel, and G. Huber, "Watt-level passively *Q*-switched Er:Lu_2O_3 laser at 2.84 μm using MoS_2," Opt. Lett. **41**, 540–543 (2016).
11. H. Uehara, S. Tokita, J. Kawanaka, D. Konishi, M. Murakami, and R. Yasuhara, "A passively *Q*-switched compact Er:Lu_2O_3 ceramics laser at 2.8 μm with a graphene saturable absorber," Appl. Phys. Express **12**, 022002 (2019).
12. Z. Yan, G. Li, T. Li, S. Zhao, K. Yang, S. Zhang, M. Fan, L. Guo, and B. Zhang, "Passively *Q*-switched Ho, Pr:$LiLuF_4$ laser at 2.95 μm using $MoSe_2$," IEEE Photon. J. **9**, 1506207 (2017).
13. R. I. Woodward, M. R. Majewski, and S. D. Jackson, "Mode-locked dysprosium fiber laser: picosecond pulse generation from 2.97 to 3.30 μm," APL Photon. **3**, 116106 (2018).
14. M. Fan, T. Li, J. Zhao, S. Zhao, G. Li, K. Yang, L. Su, H. Ma, and C. Kränkel, "Continuous wave and ReS_2 passively *Q*-switched Er:SrF_2 laser at approximately 3 μm," Opt. Lett. **43**, 1726–1729 (2018).
15. C. Kränkel, "Rare-earth-doped sesquioxides for diode-pumped high-power lasers in the 1-, 2-, and 3-μm spectral range," IEEE J. Sel. Top. Quantum Electron. **21**, 250–262 (2014).
16. T. Sanamyan, M. Kanskar, Y. Xiao, D. Kedlaya, and M. Dubinskii, "High power diode-pumped 2.7-μm Er^{3+}:Y_2O_3 laser with nearly quantum defect-limited efficiency," Opt. Express **19**, A1082–A1087 (2011).
17. H. Nie, P. Zhang, B. Zhang, M. Xu, K. Yang, X. Sun, L. Zhang, Y. Hang, and J. He, "Watt-level continuous-wave and black phosphorus passive *Q*-switching operation of Ho^{3+}, Pr^{3+}:$LiLuF_4$ bulk laser at 2.95 μm," IEEE J. Sel. Top. Quantum Electron. **24**, 1600205 (2017).
18. H. Nie, X. Sun, B. Zhang, B. Yan, G. Li, Y. Wang, J. Liu, B. Shi, S. Liu, and J. He, "Few-layer $TiSe_2$ as a saturable absorber for nanosecond pulse generation in 2.95 μm bulk laser," Opt. Lett. **43**, 3349–3352 (2018).
19. M. Fan, T. Li, S. Zhao, G. Li, X. Gao, K. Yang, D. Li, and C. Kränkel, "Multilayer black phosphorus as saturable absorber for an Er:Lu_2O_3 laser at ~3 μm," Photon. Res. **4**, 181–186 (2016).
20. A. A. Voronov, V. I. Kozlovskii, Y. V. Korostelin, A. I. Landman, Y. P. Podmar'kov, V. G. Polushkin, and M. P. Frolov, "Passive Fe^{2+}:ZnSe single-crystal *Q* switch for 3-μm lasers," Quantum Electron. **36**, 1–2 (2006).
21. H. Nie, B. Shi, H. Xia, J. Hu, B. Zhang, K. Yang, and J. He, "High-repetition-rate kHz electro-optically *Q*-switched Ho, Pr:YLF 2.9 μm bulk laser," Opt. Express **26**, 33671–33677 (2018).
22. X. Jiang, S. Liu, W. Liang, S. Luo, Z. He, Y. Ge, H. Wang, R. Cao, F. Zhang, Q. Wen, J. Li, Q. Bao, D. Fan, and H. Zhang, "Broadband nonlinear photonics in few-layer MXene $Ti_3C_2T_x$ (T = F, O, or OH)," Laser Photon. Rev. **12**, 1700229 (2018).
23. J. Koo, Y. I. Jhon, J. Park, J. Lee, Y. M. Jhon, and J. H. Lee, "Near-infrared saturable absorption of defective bulk-structured WTe_2 for femtosecond laser mode-locking," Adv. Funct. Mater. **26**, 7454–7461 (2016).
24. S. Pellegrino, L. Thomé, A. Debelle, S. Miro, and P. Trocellier, "Radiation effects in carbides: TiC and ZrC versus SiC," Nucl. Instrum. Methods Phys. Res., Sect. B **327**, 103–107 (2014).
25. M. Khazaei, M. Arai, T. Sasaki, C.-Y. Chung, N. S. Venkataramanan, M. Estili, Y. Sakka, and Y. Kawazoe, "Novel electronic and magnetic properties of two-dimensional transition metal carbides and nitrides," Adv. Funct. Mater. **23**, 2185–2192 (2013).
26. G. W. Chinthaka Silva, A. A. Kercher, J. D. Hunn, R. C. Martin, G. E. Jellison, and H. M. Meyer, "Characterization of zirconium carbides using electron microscopy, optical anisotropy, Auger depth profiles, X-ray diffraction, and electron density calculated by charge flipping method," J. Solid State Chem. **194**, 91–99 (2012).
27. A. Arya and E. A. Carter, "Structure, bonding, and adhesion at the ZrC (100)/Fe(110) interface from first principles," Surf. Sci. **560**, 103–120 (2004).
28. J. M. Dawlaty, S. Shivaraman, J. Strait, P. George, M. Chandrashekhar, F. Rana, M. G. Spencer, D. Veksler, and Y. Chen, "Measurement of the optical absorption spectra of epitaxial graphene from terahertz to visible," Appl. Phys. Lett. **93**, 131905 (2008).
29. L. Chen, C. Iwamoto, E. Omurzak, S. Takebe, H. Okudera, A. Yoshiasa, S. Sulaimankulova, and T. Mashimo, "Synthesis of zirconium carbide (ZrC) nanoparticles covered with graphitic "windows" by pulsed plasma in liquid," RSC Adv. **1**, 1083–1088 (2011).